Catalysis Science & Technology

Accepted Manuscript

ROYAL SOCIETY OF CHEMISTRY

www.rsc.org/catalysis

Catalysis Science & Technology

Catalysis Science & Technology

Dynamic Article Links ►

Cite this: DOI: 10.1039/c0xx00000x

ARTICLE TYPE

www.rsc.org/xxxxxx

Cubic *Pm*3*n* Mesoporous Aluminosilicate Assembled from Zeolite Seeds as Strong Acidic Catalysts

Tsung-Han Lin, Chia-Han Chen, Chi-Shuang Chang, Ming-Chang Liu, Shing-Jong Huang, and Soofin Cheng*

Received (in XXX, XXX) Xth XXXXXXXXX 20XX, Accepted Xth XXXXXXXXX 20XX
DOI: 10.1039/b000000x

Cubic *Pm*3*n* mesoporous aluminosilicate isomorphous to SBA-1 with 3D-interconnected pore structures was assembled by Al-incorporated zeolite seeds at pH around 9 using cetyltriethylammonium bromide as pore-directing agent. The resultant materials (termed Al-ZSBA-1) owned the advantages of strong acidity from zeolitic structures and good diffusivity of bulky reactants from 3D-interconnected mesopores. Al-ZSBA-1 with Al loading up to a Al/Si molar ratio of 0.057 still retained the cubic *Pm*3*n* structure and high surface areas (ca. 600 m^2/g). Their acidities were stronger than the counter materials prepared using sodium silicate as the silica source (referred as Al-SBA-1-alk). Moreover, all the Al(III) ions in Al-ZSBA-1 retained in tetrahedral coordination after calcination at 823 K, while a portion of Al(III) in Al-SBA-1-alk became octahedrally coordinated. In application to catalytic alkylation of 2,4-di-*tert*-butylphenol with cinnamyl alcohol, Al-ZSBA-1 gave higher flavan selectivities and yields, in comparison to Al-SBA-1-alk, ZSM-5, and beta zeolites.

1. Introduction.

Zeolites are well crystalline aluminosilicates with open structures. The materials have been widely studied and applied in oil refining and petrochemical industry as catalysts because they possess high acidity and thermal stability.[1,2] More recently, zeolites have also been utilized in fine chemicals industry.[1,3] However, the small pore sizes of less than 1.2 nm in zeolites cause slow diffusion of the bulky reactants or even block large molecules from approaching the active sites. In contrast, ordered mesoporous materials facilitate the diffusion of large molecules inside the pores and prevent the pore blockage.[4,5] Nevertheless, the mesoporous aluminosilicate materials have amorphous walls and show weaker acid strength in comparison to those of microporous zeolites.[6-9] Therefore, much efforts have been put to synthesize new types of materials, which combine the advantages of both zeolites and mesoporous molecular sieves.

The methods for the preparation of micro/mesoporous materials can be classified into five categories,[10-13] namely, (i) partial crystallization of amorphous pore walls of mesoporous silica,[14-16] (ii) using zeolite seeds as the building units of mesoporous framework,[17-22] (iii) controlled dealumination and desilication of zeolitic materials,[23-26] (iv) using carbon templating materials to incorporate mesopores during the synthesis of zeolites,[27-29] and (v) assembly of mesoporous structures with zeolitic sheets.[30] In method (i), the synthesis procedures are tedious and the ordered mesoporous structure is often destroyed in hydrothermal treatment. On the other hand, only disordered mesopores are formed by methods (iii), (iv) and (v). MCM-22 (IZA code MWW) is the first identified zeolite formed by vertically aligning lamellar zeolite intermediate.[31] The as-made MCM-22 precursor (MCM-22(P)) is the stacking of zeolitic sheets through hydrogen bond and organic template with repeating unit $d_{(001)}$ of 2.5 nm. Several methods such as calcination, delamination, swelling and pillaring have been applied to MCM-22(P) in order to generate micro/meso-porous structures namely MCM-56, MCM-36 and ITQ-2 in the past two decades.[32,33] However, the mesopores generated by pillaring or exfoliation of MCM-22(P) have wide distributed pore diameters. Recently, Ryoo's group designed a series of gemini-type, polyquaternary ammonium surfactants which could generate micropores and mesopores simultaneously, and ordered mesoporous structures (lamellar or hexagonal) with thin zeolitic walls were synthesized based on the dual-templating concept.[30,34] The drawbacks are the tedious procedure and cost in synthesizing the specially designed surfactants.

Among the mentioned methods, method (ii) using zeolite seeds as the building units of mesoporous framework has shown the advantage of facile control of the mesostructure through changing different kinds of surfactants and hydrothermal conditions. The

*Department of Chemistry, National Taiwan University, Taipei 10617, Taiwan.; TEL: +886-2-33661662; FAX: +886-2-2363-6359; E-mail: chem1031@ntu.edu.tw

mesoporous zeolite catalysts prepared by this method have been demonstrated to exhibit high catalytic activities in acid-catalyzed reactions involving large molecules.[35-37]

Among the ordered mesoporous materials, three-dimensional inter-connected pore structures are usually favorable to the one-dimensional array of pores due to better pore accessibility.[38-40] Cubic *Pm*3*n* phase SBA-1 silica with interconnected network of cage-type pores was synthesized in strong acidic media (pH << 1) with surfactants of relatively large head group ($C_nH_{2n+1}(C_2H_5)_3N^+$, n = 12, 14, 16, 18), which tend to form globular micelles.[5,41,42] The drawback of the material from practical applications has been the low stability of the as-made samples toward washing with water.[43,44] Efforts have been made to overcome this disadvantage by increasing the amount and concentration of acid used[45,46] or concomitantly adding auxiliary agents.[47] On the other hand, under the strongly acidic synthesis conditions, metal incorporation into SBA-1 framework has been very inefficient,[48-51] though the incorporation of metal ions into the framework of mesoporous silica is important in order to introduce functionalities and broaden its applications.

Our laboratory has disclosed an alkaline route to prepare well ordered cubic *Pm*3*n* silica by using sodium silicate as the silica source and cetyltriethylammonium bromide (CTEABr) as the pore-directing agent with the optimal pH value of the synthesis solution around 9.[52,53] In contrast to the conventional synthesis conditions of SBA-1, where large amount of mineral acid is needed and tetraethylorthosilicate (TEOS) was the silica source, the alkaline route is more economical and environmentally friendly. Most of all, hetero-elements could be efficiently incorporated into the silica framework through isomorphous substitution and the cubic mesostructure of the resultant material was stable toward washing with water and hydrothermal treatment.

In the present study, the effort was extended to synthesize cubic *Pm*3*n* silica assembled from aluminium substituted ZSM-5 seeds. The resultant materials were found to have higher hydrothermal stability and stronger acidic strength in comparison with the counter materials prepared from sodium silicate. The catalytic properties were examined by carrying out the alkylation of 2,4-di-*tert*-butylphenol (DTBP) with cinnamyl alcohol to form flavan as a model reaction.[53,54] Flavans are a type of flavanoids, which are a ubiquitous group of polyphenolic substances present in most plants preserving the health of plants against infections and parasites. Flavans have found numerous pharmacological applications as antioxidants,[55] antimicrobial,[56] anti-inflammatory and anti-cancer drugs.[57]

2. Experimental section

2.1 Preparation of Al(III)-incorporated Cubic *Pm*3*n* Mesoporous Silica under Alkaline Condition

Al-incorporated *Pm*3*n* mesoporous silica materials designated "xAl-SBA-1-alk", where x is the Al/Si molar percentage in the synthesis solution, were prepared referred to the procedures in reference 52. CTEABr was first dissolved in an aqueous solution containing sodium chloride and a small amount of hydrochloric acid. To this mixture at 273 K, the aqueous solution containing sodium aluminate and sodium silicate with Al/Si atomic ratios varied in 1-7% was added so that the pH value of the final solution was kept around 9. The molar composition of the reaction mixture was $Na_2SiO_3/NaAlO_2/CTEABr/NaCl/H_2O$= 1.0/0.01-0.07/0.26/6/400. After stirring for 10 min, the mixture was aged at 273 K for 24 h. The solid product was recovered by filtration, washing thoroughly with distilled water, and drying at 373 K overnight. To remove the template, the as-synthesized samples were calcined in air under static condition at 823 K for 10 h with the heating rate of 10 K/min.

2.2 Preparation of Al(III)-incorporated ZSM-5 Seeds

The ZSM-5 seeds were prepared referred to the procedures in reference 58, except all the reagents were diluted to 3.5 times to avoid the precipitation of zeolite. The solutions containing 1.5 g sodium silicate (Sigama-Aldrich, 27wt% SiO_2), 0.58 g tetrapropylammonium bromide (TPABr, Acros, 98%), 9.6 g deionized water and required amounts of $NaAlO_2$ (Hayashi Pure Chemical Ind., Ltd., 99+%) were neutralized with 1.2 M $H_2SO_{4(aq)}$ until a final pH of 11.2. After stirring at ambient temperature for 1 h, the mixture was transferred to an autoclave and heated at 423 K under static condition for different periods with various amounts of Al contents. The ZSM-5 zeolite was synthesized by the same procedure illustrated as above except that the hydrothermal time was 72 h.

2.3 Preparation of Cubic *Pm*3*n* Mesoporous Silica Assembled from Al(III)-incorporated ZSM-5 Seeds

The procedures were similar to those for preparation of Al-SBA-1-alk, except Al(III)-incorporated ZSM-5 seeds were used as the silica and aluminium sources. In a typical procedure, 0.712 g CTEABr was dissolved in the aqueous solution containing 2.32 g sodium chloride (Acros, 99.5%), a appropriate amount of hydrochloric acid and 40 g H_2O. After stirring for 120 min at room temperature, this mixture was cooled down to 273 K in ice bath and stirred for 60 min. Then, ZSM-5 seed solution was added to this mixture under stirring. The molar composition of the final mixture was Na_2SiO_3/ $NaAlO_2$/TPABr/CTEABr/ NaCl/ H_2O = 1.0/0.01~0.07/0.32/ 0.26/ 6/ 400. After stirring for 10 min, the mixture was aged under static condition at 273 K for 24 h. The solid product was recovered by filtration, washing thoroughly with deionized water, and drying at 373 K overnight. To remove the template, the as-synthesized samples were calcined in air under static conditions at 823 K for 10 h with the heating rate of 10 K/min. The resultant materials are designated "xAl-ZSBA-1", where x is the Al/Si molar percentage in the synthesis solution.

2.4 Characterization

Powder X-ray diffraction (XRD) patterns were recorded using a PANalytical X'pert Pro diffractometer with Cu *K*α radiation operated at 40 mA and 45 kV. N_2 adsorption-desorption isotherms were measured using a Micromeritics Tristar 3000 system at liquid nitrogen temperature (77 K). Before the measurements, the samples were degassed at 473 K for 10 h under vacuum condition (10^{-3} torr). The surface area was calculated by using Brunauer-Emmett-Teller (BET) method. Pore size was determined by Barrett-Joyner-Halenda (BJH) method using the desorption branch of the isotherms. Transmission electron microscopy (TEM) was performed on a JEOL JEM-1200EX II Transmission Electron Microscope, operating at 80

kV, and the scanning electron microscopy (SEM) images were taken using a cold-field emission Scanning Electron Microscope (Hitachi S-4800). The ^{29}Si and ^{27}Al NMR experiments were carried out at frequencies of 59.63 and 78.21 MHz, respectively, on a Brucker MSL-300 NMR spectrometer equipped with a commercial 7 mm MAS-NMR probe. The magic-angle spinning frequencies were set to 5 kHz for all experiments. Chemical shifts were externally referenced to $Si(CH_3)_4$ and 1M $Al(NO_3)_3$ solution. The $Q^4/(Q^2+Q^3)$ area ratios were obtained by deconvolution of the peaks in the spectra using WinFit software. The inductively coupled plasma-mass spectrometry (ICP-MS) of the samples dissolved in diluted HF aqueous solutions were taken by using an Agilent 7700e ICP/MS instrument. Temperature-programmed desorption of ammonia (NH_3-TPD) was performed by a Micrometrics Autochem 2910 system equipped with a thermal conductivity detector (TCD). Prior to the measurements, the samples (ca. 300 mg) were pre-treated at 823 K for 1 h under a He flow to eliminate physically adsorbed water. The samples cooled to 373 K and then adsorbed NH_3 for 30 min, followed by purging with He gas again for another 30 min to eliminate physically adsorbed ammonia. The NH_3-TPD profiles were measured over the temperature range of 373-823 K by using He as a carrier gas of 30 mL/min. Prior to each FT-IR experiment, compressed sample placed in the IR cell (with ZnSe windows) was first subjected to evacuation treatment at 673 K for 3 h, followed by cooled down to room temperature and then saturated adsorption of pyridine for 0.5 h and subsequent removal of physisorbed pyridine under vacuum overnight. Each FT-IR spectra was acquired by scanning from 4000 to 400 cm^{-1}; 32 repeated scans were accumulated. The accessibility of Brønsted acid sites in the materials was determined by ion-exchange with cations of various sizes followed by acid-base titration. Aqueous solutions of sodium chloride (NaCl, 2 M), tetramethylammonium chloride (TMACl, 0.05 M), and tetrabutylammonium bromide (TBABr, 0.05 M) were used as the exchange agents. In a typical experiment, 0.20 g of the solid was first dried at 200 °C for 1 day and then added to 40 mL of aqueous solution containing the corresponding salt. The suspension was mixed to reach equilibrium for 6 h, then the solid was filtered and washed with a small amount of water. Finally, the filtrate was titrated by 0.01 M aqueous solution NaOH.

2.5 Catalytic Reaction Procedure

To generate Brønsted acid sites on Al-SBA-1-alk and Al-ZSBA-1, the calcined samples were ion-exchanged with 1 M NH_4Cl aqueous solution twice, followed by filtration, washing with de-ionized water, drying at 373 K and calcination again at 823 K. Before catalytic test, the catalyst was baked at 473 K at least for 5 h to remove adsorbed moisture. The alkylation of DTBP with cinnamyl alcohol was performed in a 50 mL flask immersed in a thermostat bath with a magnetic stirrer. 100 mg of the catalyst suspended in 12.5 mL solvent was mixed with 0.25 mmol of DTBP (Aldrich, 98%) and 0.25 mmol of cinnamyl alcohol (Aldrich, 97%), and the reaction was proceeded at 368 K for different reaction periods. After quenching the reaction by cooling at room temperature, the liquid products were separated from the solid catalyst by filtration and analyzed by a Shimadzu GC-2014 gas chromatograph (GC) equipped with a flame ionization detector (FID) and a RTX-5 capillary column (30 m*0.53 mm) using octane (Acros, 99+%) as an internal standard. The selectivities of alkylation products, 2,4-di-*tert*-butyl-6-cinnamylphenol (DTBCP) and flavan were determined by assuming both compounds have the same FID response factors, because pure DTBCP was not commercially available.

3. Results and discussion

Fig. 1 shows the XRD patterns of the calcined materials prepared at pH 9. The XRD patterns of the calcined Al-ZSBA-1 samples show three distinct diffraction peaks at 2θ~1.5−2.5° indexed to the (200), (210), and (211) planes of cubic *Pm*3*n* symmetry, and also some weaker diffraction peaks at 2θ~3−4° assigning to the (222), (320), (321), and (400) planes.[59] The calcined Al-ZSBA-1 samples with Al/Si molar percentages lower than 5% still retain three resolvable diffraction peaks at 2θ~1.5-2.5°, while the one synthesized with Al/Si = 7% has only a broad peak in this region. These results imply that the well-ordered mesopores in cubic *Pm*3*n* arrangement can be retained with the Al/Si molar ratio up to 5% in the synthesis solution. It is also noticed that no separated zeolite phase was formed since no diffraction peaks corresponding to ZSM-5 structure were detected in the high angle regions (as shown in the inserted figures). On the other hand, the counter samples synthesized using sodium silicate instead of zeolite seeds as the silica source lose the resolvable diffraction peaks at 2θ~1.5–2.5° when the Al/Si molar percentages are only higher than 3%.

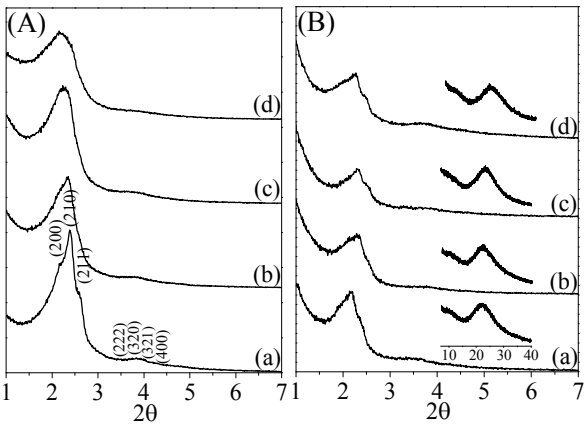

Fig. 1 XRD patterns of calcined (A) Al-SBA-1-alk, (B) Al-ZSBA-1 with various Al/Si molar ratios: (a) 1%, (b) 3%, (c) 5%, and (d) 7%.

The textural properties of the calcined Al-SBA-1-alk and Al-ZSBA-1 samples were examined by N_2 physisorption experiments, and the results are shown in Fig. 2 and Table 1. All the calcined samples have type IV isotherms according to the IUPAC classification, and that was the characteristics of ordered mesoporous materials. They are basically in the shape similar to that of conventional SBA-1 prepared in acidic condition. The surface areas and pore volumes of Al-SBA-1-alk are 900−1100 m^2/g and 0.75−0.82 cm^3/g, respectively. In comparison, the surface areas of Al-ZSBA-1 samples are lower (600−800 m^2/g). It is also noticeable that Al-ZSBA-1 samples contain small amounts of microporous volumes while Al-SBA-1-alk samples do not.

SEM images show that both Al-ZSBA-1 and Al-SBA-1-alk materials are generally spherical without any facets (Fig. 3). The particle sizes of the materials synthesized in alkaline condition

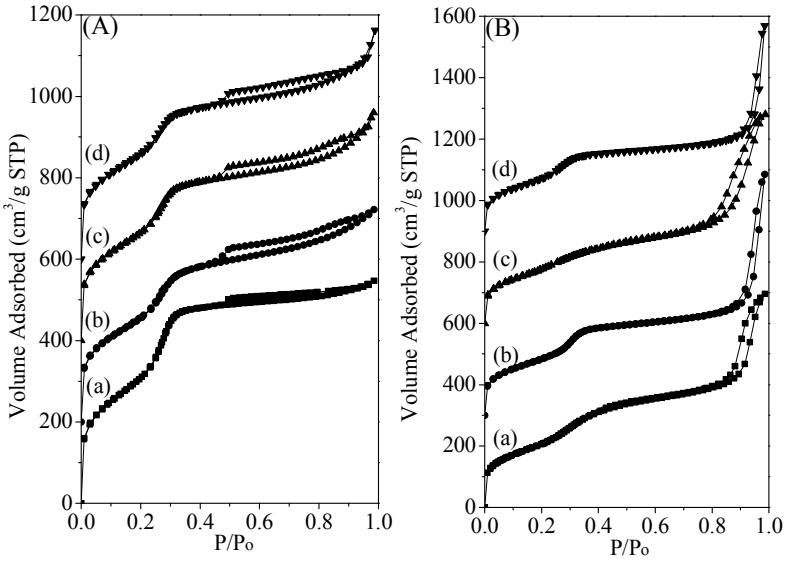

Fig. 2 N_2 adsorption-desorption isotherms of (A) Al-SBA-1-alk and (B) Al-ZSBA-1 samples with various Al/Si molar ratios: (a) 1%, (b) 3%, (c) 5%, and (d) 7%. Profiles are shifted in vertical axis by 200 cm^3/g STP between profiles in (A) and by 250 cm^3/g STP in (B).

Table 1 Physicochemical properties of calcined cubic Pm3n mesoporous silica samples prepared with various amounts of Al at alkaline condition.

Sample	d_{210} (nm)	S_{BET} (m^2/g)	D_p (nm)[a]	V_{total} (cm^3/g)	V_{micro} (cm^3/g)[b]	FWHM (ppm)[c]
1Al-SBA-1-alk	3.6	1148	2.2	0.82	0	17.5
3Al-SBA-1-alk	3.8	945	2.2	0.77	0	18.1
5Al-SBA-1-alk	4.0	982	2.2	0.79	0	17.6
7Al-SBA-1-alk	4.1	961	2.2	0.75	0	16.6
1Al-ZSBA-1	4.1	759	2.4	0.86	0.03	15.7
3Al-ZSBA-1	3.8	677	2.4	0.70	0.02	15.4
5Al-ZSBA-1	3.8	652	2.4	0.66	0.05	15.8
7Al-ZSBA-1	3.9	645	2.4	0.60	0.07	15.2

[a] Calculated from desorption branch; [b] Calculated from t-plot method; [c] Solid-state ^{27}Al MAS NMR peak at 50 ppm.

vary in a large range from 0.1 to 1 μm in diameter. They are different from the particles of SBA-1 synthesized by acidic route, which have well-defined external morphology with crystal facets and the particle sizes in 3-15 μm.[60,61] The smaller particle sizes of the materials synthesized in alkaline conditions are due to the faster precipitation rate of the silica.[52] It is also noticeable that the particle sizes decrease with the increase in Al content. Al atoms in the synthetic solution probably act as nuclei for material growth, and larger amount of nuclei leads to faster precipitation and smaller particle size. On the other hand, the particle sizes of Al-ZSBA-1 samples are less homogeneous than those of Al-SBA-1-alk. Large amounts of agglomerates of nano-particles can be seen on Al-ZSBA-1 materials as the Al content increases, and that accounts for the abrupt increases in N_2 sorption at high P/P_0 region in the N_2 sorption isotherms observed in Fig. 2(B). The TEM photographs shown in Fig. 4 confirm that the Al-SBA-1-alk and Al-ZSBA-1 materials possessed long-range ordering of the 3D cubic arrays. The average pore diameter determined from TEM photographs is around 2 nm, which is in consistence with that from N_2 sorption experiments.

Fig. 5 shows the FT-IR spectra of calcined Al-SBA-1-alk and Al-ZSBA-1 samples in comparison to that of ZSM-5. The peaks near 450, 800, 1100, and 1220 cm^{-1} are assigned to the Si-O-Si bending and stretching vibrations of condensed silica framework. According to the Flanigen-Khatami-Szymanski correlation,[62,63] these peaks are corresponding to internal vibration of $Si(A1)O_4$ tetrahedra and are common to silica and quartz. For the cubic *Pm3n* silica materials, these peaks are relatively broader in comparison to those of ZSM-5 due to the amorphous nature of the silica framework. In addition, a bending vibration of non-

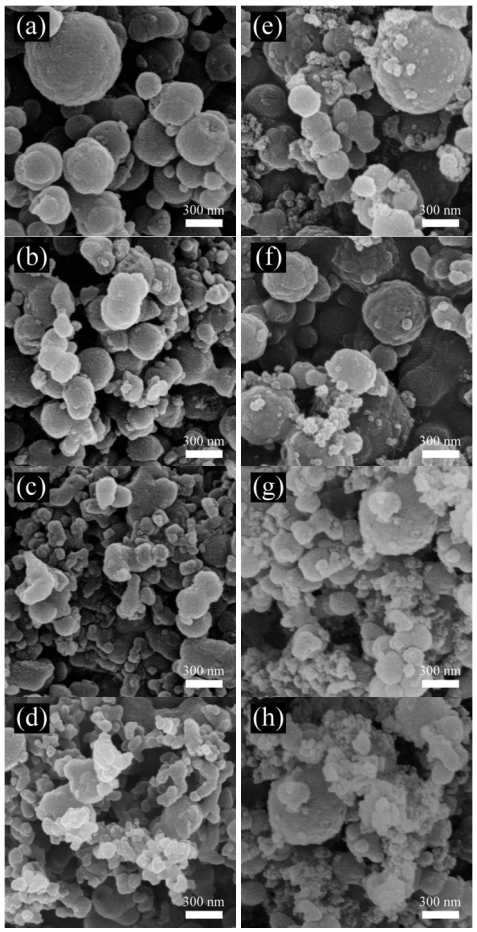

Fig. 3 SEM photographs of Al-SBA-1-alk (a-d) and Al-ZSBA-1 (e-h) samples with various Al/Si molar ratios: (a, e) 1%, (b, f) 3%, (c, g) 5%, (d, h) 7%.

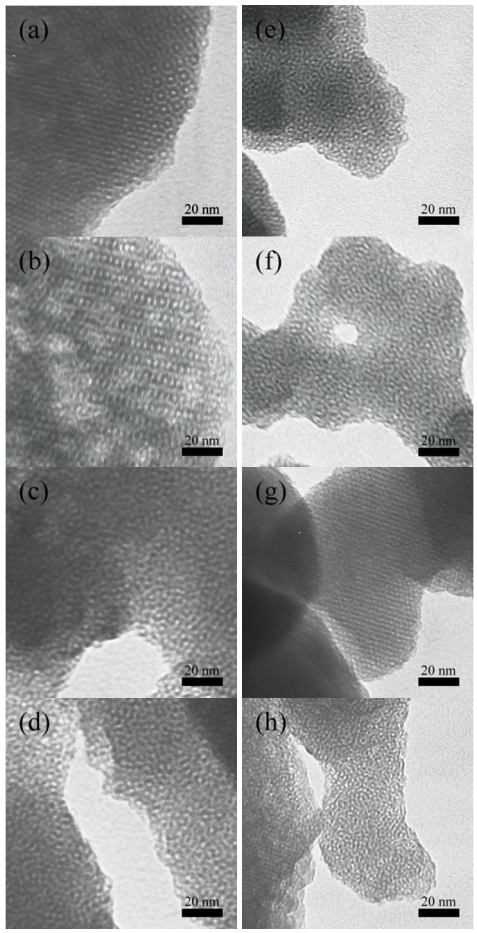

Fig. 4 TEM photographs of Al-SBA-1-alk (a-d) and Al-ZSBA-1 (e-h) samples with various Al/Si molar ratios: (a, e) 1%, (b, f) 3%, (c, g) 5%, (d, h) 7%.

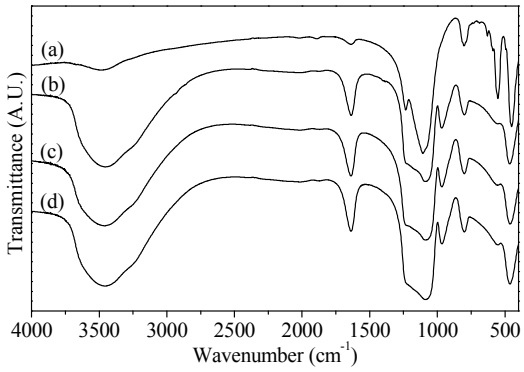

Fig. 5 FT-IR spectra of (a) ZSM-5, (b) 2Al-SBA-1-alk, (c) 2Al-ZSBA-1 and (d) 5Al-ZSBA-1.

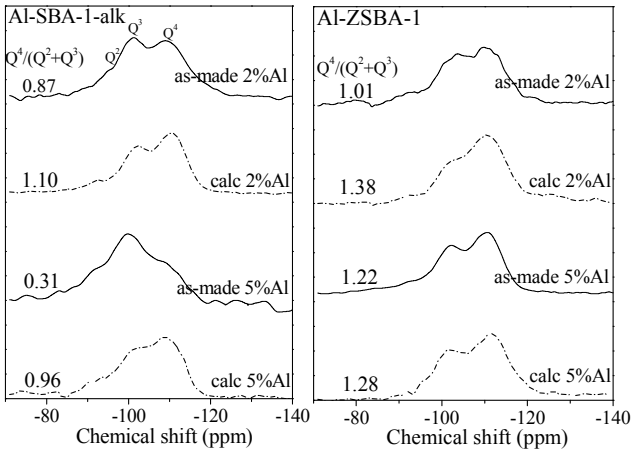

Fig. 6 Solid state ^{29}Si MAS NMR of Al-SBA-1-alk and Al-ZSBA-1 before and after calcination.

condensed silanol group appears at ca. 960 cm^{-1} and the bending and stretching vibrations of hydroxyl groups and physically adsorbed water appear at 1650 and 3450 cm^{-1}, respectively. It is noticeable that the walls of both Al-SBA-1-alk and Al-ZSBA-1 materials contain large amounts of silanol groups, akin to amorphous silica. The absorption at 550-650 cm^{-1}, on the other hand, was assigned to the presence of a double-ring of tetrahedra in the zeolitic framework.[64,65] For a ZSM-5 structure, the latter absorption appears near 550 cm^{-1}. The intensity ratio of the peaks at 550 to 450 cm^{-1} is often used as a quantitative measurement of zeolite crystallinity. The ratio for the ZSM-5 sample is 0.77, and the Al-ZSBA-1 materials have the ratios of 0.61–0.63, which are only slightly higher than 0.58 for 2Al-SBA-1-alk. These results imply that the zeolite seeds incorporated in the walls of Al-ZSBA-1 materials have low crystallinity.

The solid state ^{29}Si MAS NMR spectra of the as-made and calcined Al-SBA-1-alk and Al-ZSBA-1 samples were shown in Fig. 6 Two distinct resonance peaks at -100 and -110 ppm

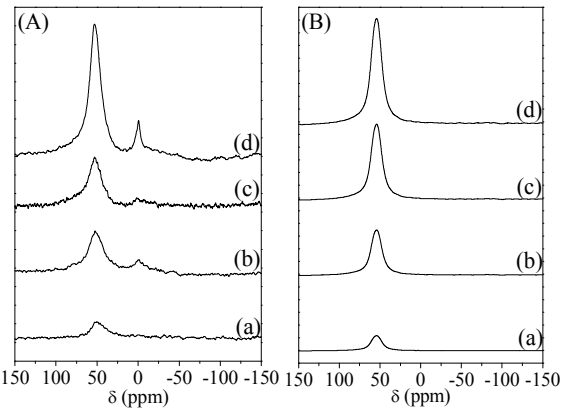

Fig. 7 Solid state ^{27}Al MAS NMR spectra of calcined (A) Al-SBA-1-alk, (B) Al-ZSBA-1 with various Al/Si molar ratios: (a) 1%, (b) 3%, (c) 5%, and (d) 7%.

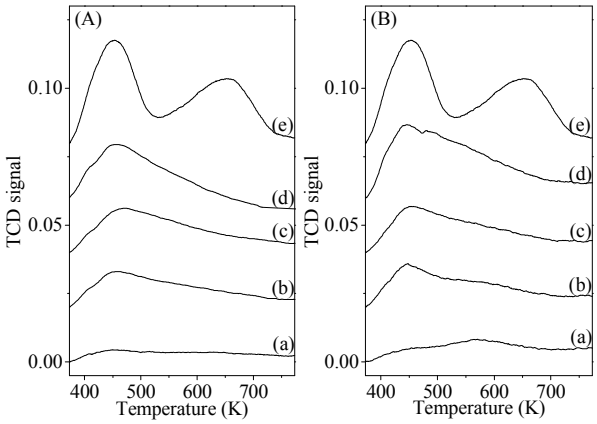

Fig. 8 NH_3-TPD profiles of calcined (A) Al-SBA-1-alk, (B) Al-ZSBA-1 with various Al/Si molar ratios: (a) 1%, (b) 3%, (c) 5%, (d) 7%, and (e) ZSM-5.

corresponding to Q^3 and Q^4, respectively, as well as a weak shoulder at -91 ppm for Q^2 are clearly seen, where Q^n represents Si in different coordination environments of $Si(OSi)_n(OH)_{4-n}$ or $Si(OSi)_n(OAl)_{4-n}$ and n= 2–4. The relative integrated intensities of the $Q^4/(Q^2+Q^3)$ signals for the as-made Al-ZSBA-1 samples are higher than those of as-made Al-SBA-1-alk samples, implying that the silicate condensation is more complete when zeolite seeds instead of sodium silicate were used as the silica source. The degree of silicate condensation was further increased when these samples were calcined at 823 K for 6 h.

Fig. 7 shows the solid state ^{27}Al MAS NMR spectra of the calcined samples containing various amounts of Al(III). All the Al-ZSBA-1 samples show only a single peak at 50 ppm, assigning to the tetrahedrally coordinated aluminium. Moreover, the peak intensity increases with the aluminium content. The absence of signals around 0 ppm, which corresponds to Al(III) ions in octahedral coordination, indicates that no extra-framework alumina species were formed. In contrast, the Al-SBA-1-alk samples with Al/Si molar ratios in the synthesis solutions higher than 3% have an additional small peak appeared at 0 ppm in the ^{27}Al MAS NMR spectra. Extra-framework alumina species are probably formed in these Al-SBA-1-alk samples. These results imply that the Al(III) ions are better retained in the tetrahedral sites of the mesoporous silica framework if they are incorporated into the zeolite seeds first. In addition, the value of full width at half maximum (FWHM) for the Al tetrahedral peaks provides a measurement of the uniformity of Al microenvironment in both zeolites and amorphous silicas.[37,66] For the Al-ZSBA-1 samples, the FWHM values are all around 15 ppm and smaller than those of Al-SBA-1-alk samples (Table 1). This result clearly evidences that using zeolite seeds as silica source can increase the uniformity of Al environment in the mesoporous materials.

The acidities of the calcined Al-ZSBA-1 samples were compared with those of Al-SBA-1-alk and ZSM-5 by carrying out the NH_3-TPD experiment, and the profiles were shown in Fig. 8. ZSM-5 owns the largest acid amount and strongest strength among the studied materials. Two strong and broad signals with the maxima appeared at 484 and 706 K, indicating that there are two kinds of acid sites in ZSM-5. In contrast, the Al-ZSBA-1 materials have only one signal covering 373–700 K with the maximum at ca. 450 K. Moreover, the Al-SBA-1-alk materials have similar NH_3-TPD profiles as that of Al-ZSBA-1. However, the Al-ZSBA-1 materials have one shoulder peak at ca.573 K, indicating that the Al-ZSBA-1 materials contain extra portions of stronger acidic sites in comparison to Al-SBA-1-alk.

The nature of acidic sites on these porous materials was examined by taking FT-IR spectra of the samples after pyridine adsorption, and the results are shown in Fig. 9. The Lewis and Brønsted acid sites are characterized by the pyridine ring stretching vibrations appeared at 1454 and 1545 cm^{-1}, respectively.[67-69] The relative intensity ratio of these two peaks was found to vary with different samples. The 1545 cm^{-1} peak for 5Al-ZSM-5 is much stronger than 1456 cm^{-1} peak, indicating that 5Al-ZSM-5 has larger amount of Brønsted acid sites than Lewis acid sites. Although the intensity of both peaks decrease with desorption temperature, they are still detectable after desorption treatment at 673 K. In comparison, 5Al-SBA-1-alk and 5Al-ZSBA-1 both have 1454 and 1545 cm^{-1} peaks in similar intensity at 373 K, and the 1454 cm^{-1} peak becomes dominant as the desorption temperature increases, implying that the mesoporous materials contain relatively large amounts of Lewis acid sites. Moreover, small peaks are still retained at 1454 and 1545 cm^{-1} for 5Al-ZSBA-1 after desorption treatment at 673 K, while they almost disappear for 5Al-SBA-1-alk. These results demonstrate that the acidic strength of 5Al-ZSBA-1 is higher than 5Al-SBA-1-alk. The ratios of Brønsted/Lewis acidic sites, based on the FT-IR peak areas, are listed in Table 2. 5Al-ZSM-5 has a ratio of 2.1, which is twice higher those of 5Al-ZSBA-1 (0.9) and 5Al-SBA-1-alk (0.6). Nevertheless, the acidic property of 5Al-ZSBA-1 materials is between those of 5Al-ZSM-5 and 5Al-SBA-1-alk.

The accessibility of acidic sites in the Al-containing porous samples was studied by ion-exchange of the protons on the Brønsted acidic sites with cations of different sizes and the exchange capacities were determined by titrating the filtrate with NaOH aqueous solution.[70,71] The results are also shown in Table 2. The exchange capacities of all samples decreased when the size of ion-exchange agent became bigger. For 5Al-ZSM-5 sample, the exchange capacity with Na^+ is 0.67 mmol/g, which is ca. 80% of Al content. This ratio is almost the same as the ratio of Brønsted acid site determined by IR spectra of adsorbed pyridine versus tetrahedral Al content determined by NMR reported by Datka et al.[72] The exchange capacity with TMA^+ is slightly lower (0.62 mmol/g) and that with TBA^+ decreases abruptly to 0.11

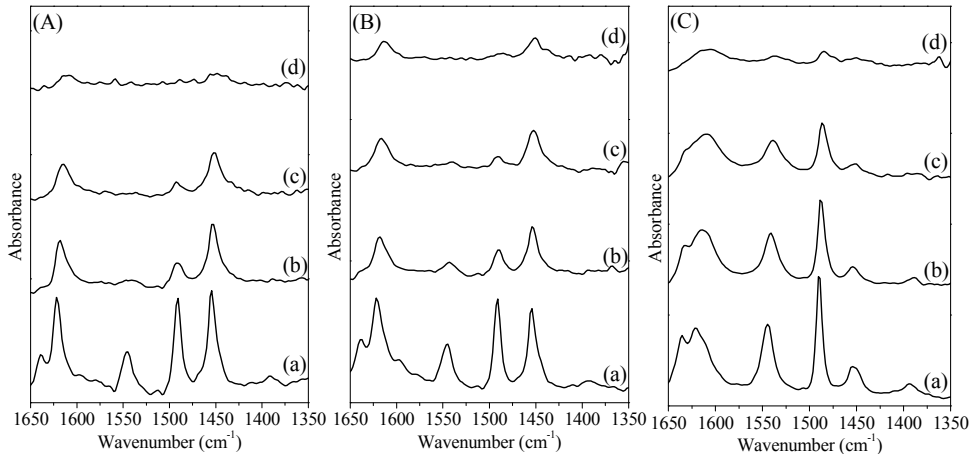

Fig. 9 The FT-IR spectra of calcined (A) 5Al-SBA-1-alk, (B) 5Al-ZSBA-1 (C) 5Al-ZSM-5 after pyridine adsorption and then desorption at different temperatures: (a) 373 K, (b) 473 K, (c) 573 K, (d) 673 K.

Table 2 Al contents and cation-exchange capacities of various samples

Sample	Al content ($mmol/g_{cat}$)[a]	Exchange capacity ($mmol/g_{cat}$)			Ratio of accessibility[b]	Ratio of B/L acid[c]	Ratio of B/L acid[d]
		Na^+	TMA^+	TBA^+			
5Al-ZSM-5	0.84	0.67	0.62	0.11	16%	3.9	2.1
5Al-SBA-1-alk	0.92	0.51	0.50	0.47	92%	1.2	0.6
5Al-ZSBA-1	0.80	0.50	0.48	0.41	82%	1.7	0.9

[a] Measured by ICP-MS; [b] Calculated from the ratio of exchange capacities (TBA^+/Na^+); [c] Calculated from ion-exchanged method; [d] Calculated from pyridine adsorption-desorption FT-IR spectra.

mmol/g. The ratio of TBA^+/Na^+ exchange capacities is 16%. These results indicate that the micropore diameter of ZSM-5 is too small to accommodate TBA^+ ions. On the other hand, both mesoporous SBA-1 samples have Na^+ exchange capacities around 0.5 mmol/g, which is ca. 55% and 62% of Al contents in 5Al-SBA-1-alk and 5Al-ZSBA-1, respectively. Since Na^+ ions should exchange with Brønsted acidic sites only, the difference between Al content and Na^+ exchange capacity should be the content of Lewis acidic sites. The ratios of Brønsted/Lewis acidic sites, calculated from Na^+ ion-exchange, are shown in Table 2. 5Al-ZSM-5 has a ratio of 3.9, which is much higher than those of 5Al-ZSBA-1 (1.7) and 5Al-SBA-1-alk (1.2). It is reported that the ratios of Brønsted/Lewis acidic sites on Al-SBA-15 which has 2D hexagonal structure are ca. 0.5 and much lower than those of zeolites.[73] Our results show that Al-SBA-1 has higher ratios of Brønsted/Lewis acidic sites than Al-SBA-15, but lower than ZSM-5. The proportion of the Brønsted/Lewis acidic ratios of 5Al-ZSM-5, 5Al-SBA-1-alk and 5Al-ZSBA-1 is 3.3: 1: 1.4, which is very similar to the proportion of 3.5: 1: 1.5, calculated from pyridine adsorption FT-IR spectra. These results demonstrate that the ion-exchange method is as reliable as pyridine adsorption FT-IR spectra in determining the ratio of Brønsted/Lewis acidic sites on the sample.

For 5Al-SBA-1-alk samples, the exchange capacities only decreases slightly when the size of exchange agent increases from Na^+ to bulky TBA^+. In comparison, more significant decrease is seen on 5Al-ZSBA-1 sample. The ratios of TBA^+/Na^+ exchange capacities are 92% and 82% for 5Al-SBA-1-alk and 5Al-ZSBA-1, respectively. These results confirmed that most of the Brønsted acidic sites on mesoporous SBA-1 materials are accessible by bulky TBA^+ ions. However, the 5Al-ZSBA-1 sample has ca. 10% of the acidic sites probably buried inside the micropores of zeolite seeds and not accessible by bulky TBA^+ ions.

4. Catalytic alkylation of DTBP by cinnamyl alcohol

The Friedel-Crafts alkylation of DTBP with cinnamyl alcohol and the subsequent isomerization of DTBCP to yield flavan (Scheme 1) in the liquid phase were chosen as a model reaction to evaluate the catalytic activities of Al-containing cubic *Pm*3*n* mesoporous silica. This is a challenging catalytic reaction. The first step of alkylation is a Friedel-Crafts reaction and needs

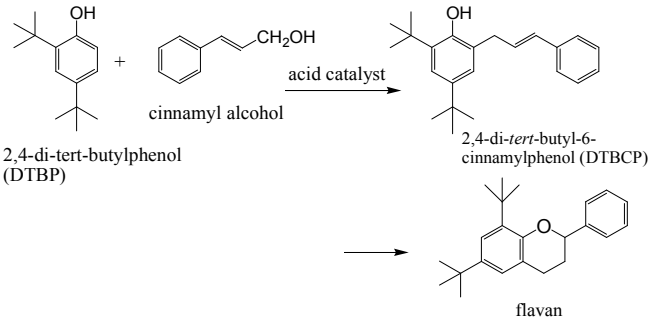

Scheme 1 Reaction paths of alkylation of DTBP with cinnamyl alcohol to form flavan.

Table 3 Alkylation of DTBP with cinnamyl alcohol over homogeneous acid catalysts

Catalyst	DTBP conv. (%)	Cinnamyl alcohol conv. (%)	Flavan Select. (%)	Flavan yield (%)	DTBCP yield (%)
H_2SO_4	0	100	0	0	0
CH_3COOH	0	0	0	0	0

[a] Reaction conditions: 0.25 mmol DTBP, 0.25 mmol cinnamyl alcohol, 10 mg 35% H_2SO_4 or 6 mg acetic acid, 12.5 mL isooctane, 368 K, 5 h

relatively strong acids to catalyze the reaction, while the second isomerization reaction can be catalyzed by a relatively weak acid. Moreover, there are several competitive reactions (as shown in Scheme 2). To demonstrate this point, we have used sulfuric acid and acetic acid containing similar acid amounts as the solid catalysts to representing the strong and weak acids in catalyzing the reaction in homogeneous system under the same reaction condition as that over solid catalysts. The results are summarized in Table 3. When using H_2SO_4 as the catalyst, the only reaction products obtained are the oligomers and polymers formed by cinnamyl alcohol. It implies that polymerization of cinnamyl alcohol is favorable to Friedel-Crafts reaction over strong acids. On the other hand, no reaction was observed over acetic acid. Therefore, the medium acid strength of zeolite and mesoporous silica is most suitable for catalyzing this reaction.

Table 4 compares several solvents commonly used in the literature for the catalytic reaction. Among them, isooctane and dimethylacetamide (DMAc) could reach a reaction temperature of 368 K, while acetonitrile (ACN) could only reach 355 K due to its relatively lower boiling point. The highest DTBP conversion and flavan yield were observed in isooctane. In contrast, no catalytic activity was seen using DMAc of a high dielectric constant of 37.8 as the solvent. It is attributed to that DMAc of high polarity and also as a weak base (pKa of its conjugate acid around -0.5) will hinder the reaction by adsorbing strongly on the catalytic active sites. On the other hand, the catalyst gave a lower DTBP conversion and DTBCP yield using acetonitrile as solvents than isooctane, but no flavan was formed. It is attributed to that the isomerization of DTBCP to flavan is an endothermic reaction and unfavorable at low reaction temperature. Consequently, isooctane is the most suitable solvent among the studied solvents, and it is used hereafter.

Fig. 10 shows the DTBP conversion and product yields over 5Al-SBA-1-alk catalyst as a function of reaction period. In the first 10 min, two different reactions proceed simultaneously. One is Friedel-Crafts alkylation of DTBP with cinnamyl alcohol to

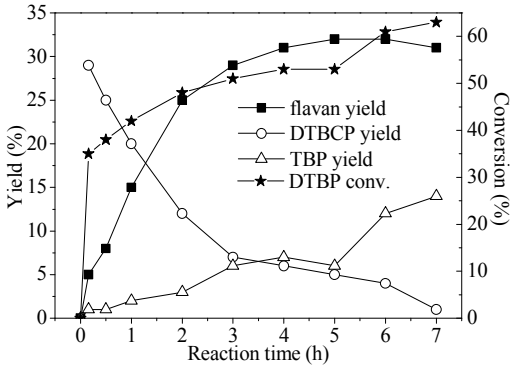

Fig. 10 The DTBP conversion and the product yield as a function of reaction time. (■: flavan yield, ○: transcinnamlphenol yield, △: TBP yield, and ★: DTBP conversion)

form DTBCP, and the other is polymerization of cinnamyl alcohol to form oligomers or polymers.[74] The cinnamyl alcohol was found to be completely consumed in 10 min., while the DTBP conversion is only 35% at this stage. This result indicates that the polymerization of cinnamyl alcohol is still faster than Friedel-Crafts alkylation over 5Al-SBA-1-alk catalyst. After the consumption of cinnamyl alcohol, the DTBP conversion still increases steadily with reaction time. It is due to the proceeding of transalkylation between DTBP molecules. As a result, *tert*-butylphenol (TBP) and 2,4,6-tri-*tert*-butylphenol (TTBP) are formed as the side products.

The main product in the liquid phase at 10 min is DTBCP formed through Friedel-Crafts alkylation of DTBP with cinnamyl alcohol. The yield of DTBCP then decreases with reaction time due to the isomerization of DTBCP to form flavan through Michael reaction. All DTBCP are converted to flavan, and theflavan yield reaches maximum after 5 h of reaction. All the reaction pathways are illustrated in Scheme 2.

The effect of reaction temperature on the catalytic results over 5Al-SBA-1-alk is shown in Table 5. The DTBP conversion increases with reaction temperature. Moreover, the flavan selectivity reaches 60% at 368 K, but no flavan product is formed at low reaction temperature of 333 K. This result is attributed to that the isomerization of DTBCP to flavan is an endothermic reaction. It is also noticeable that the total yields of flavan and DTBCP maintain around 37% and do not change significantly with the reaction temperature. The increased conversion of DTBP at higher temperatures is thus contributed by transalkylation reaction between DTBP molecules. It is to say that transalkylation reaction is also an endothermic reaction.

In order to minimize the consumption of cinnamyl alcohol in polymerization reaction, the amount of cinnamyl alcohol in

Table 4 Alkylation of DTBP with cinnamyl alcohol with different solvents

Solvent	Rxn temp.(K)	Dielectric constant	DTBP conv. (%)	Flavan select. (%)	Flavan yield (%)	DTBCP yield (%)	TBP yield (%)
Isooctane	368	1.94	53	60	32	5	6
DMAc	368	37.8	<1	0	0	0	0
ACN	355	37.5	20	0	0	18	0

[a] Reaction conditions: 0.25 mmol DTBP, 0.25 mmol cinnamyl alcohol, 125 mg catalyst (5Al-SBA-1-alk), 12.5 mL solvent, 5 h.

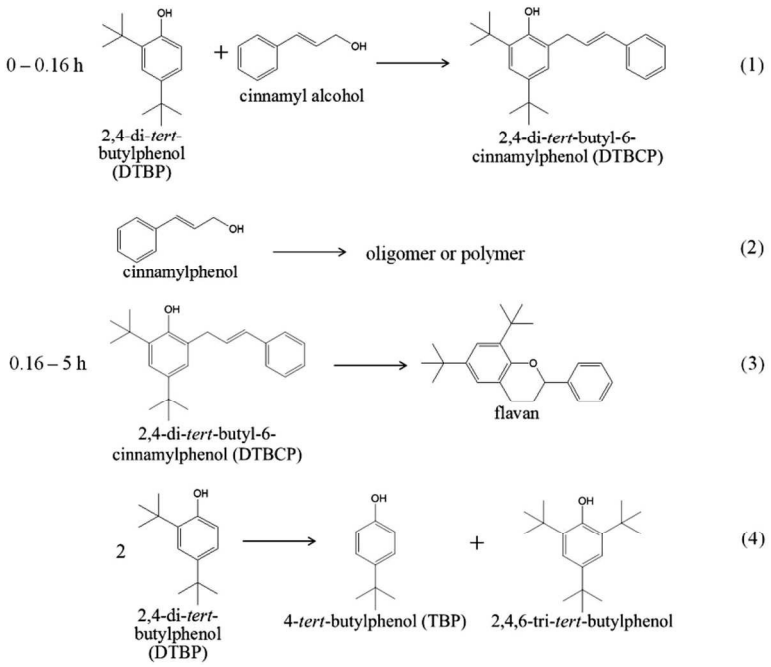

Scheme 2 Reactions proceeded in different periods

Table 5 Alkylation of DTBP with cinnamyl alcohol with different reaction temperature

Reaction temp. (K)	DTBP conv. (%)	Flavan select. (%)	Flavan yield (%)	DTBCP yield (%)	TBP yield (%)
333	34	0	0	35	0
353	43	24	10	29	0
368	53	60	32	5	6

[a] Reaction conditions: 0.25 mmol DTBP, 0.25 mmol cinnamyl alcohol, 125 mg catalyst (5Al-SBA-1-alk), 12.5 mL isooctane, 5 h.

Table 6 Alkylation of DTBP with cinnamyl alcohol with different molar ratios of DTBP/cinnamyl alcohol

DTBP/ cinnamyl alcohol	DTBP conv. (%)	Flavan select. (%)	Flavan yield (%)	DTBCP yield (%)	TBP yield (%)
0.5	39	13	5	35	0
1	53	60	32	5	6
2	61	51	31	0	13

[a] Reaction conditions: 0.25 mmol DTBP, 0.125-0.5 mmol cinnamyl alcohol, 125 mg catalyst (5Al-SBA-1-alk), 12.5 mL isooctane, 368 K, 5 h.

reactants was reduced. Table 6 shows that DTBP conversion indeed increases with increasing the molar ratio of DTBP/cinnamyl alcohol. However, the flavan yield reaches the maximum when the molar ratio of DTBP/cinnamyl alcohol is 1. If the DTBP/cinnamyl alcohol ratio increases to 2, products of transalkylation reaction between DTBP molecules also increase. Therefore, an equimolar mixture of DTBP and cinnamyl alcohol is the optimal ratio of the reactants for this reaction.

Table 7 compares the Al contents and catalytic activities of Al-ZSBA-1 and Al-SBA-1-alk materials with those of ZSM-5 and Beta zeolites. Elemental analyses by ICP-MS show that the amounts of Al(III) ions incorporated in either Al-ZSBA-1 or Al-SBA-1-alk were close to those in the synthesis solutions up to Al/Si atomic ratio of 5%. Nevertheless, the Al contents in Al-SBA-1-alk materials are slightly higher than those of Al-ZSBA-1, except those of lowest Al contents, saying samples 1Al-ZSBA-1 and 1Al-SBA-1-alk.

The DTBP conversions over all the Al-SBA-1-alk materials are higher than those over Al-ZSBA-1. Since even 1Al-SBA-1-alk, which has lower Al content than 1Al-ZSBA-1, has higher DTBP conversion than 1Al-ZSBA-1, it is probably because of the relatively higher surface areas of Al-SBA-1-alk materials. However, the flavan selectivities over Al-ZSBA-1 materials are higher than those over Al-SBA-1-alk. These results demonstrate that the Al-ZSBA-1 materials can catalyze the Michael reaction more efficiently than mesoporous materials of amorphous walls. Moreover, the flavan selectivities over Al-ZSBA-1 materials are similar to that over ZSM-5, except 1Al-ZSBA-1 which has lowest acidity. This is an indication that Al-ZSBA-1 materials own strong acidities from the zeolite seeds incorporated on the pore walls. On the other hand, the TOF, which was calculated as conversion of DTBP molecule per Al atom per hour, decreases with the increase in Al loading for both Al-SBA-1-alk and Al-ZSBA-1 materials, indicating that a portion of aluminium may be buried inside the silica framework and not accessible by the reactants. Nevertheless, higher TOFs are obtained over the mesoporous Al-SBA-1-alk and Al-ZSBA-1 catalysts in comparison to those of microporous zeolites of similar Al contents, inferring that the large mesopores of cubic *Pm*3*n* silica should facilitate the bulky reactant and intermediate molecules to diffuse and access the acidic sites inside the pores. In contrast, the zeolites give relatively low conversions due to its pore sizes of

Table 7 Alkylation of DTBP with cinnamyl alcohol over Al-SBA-1-alk and Al-ZSBA-1 with different Al-loadings.

Sample	Al/Si[a] (%)	DTBP conv. (%)	Flavan select. (%)	Flavan yield (%)	DTBCP yield (%)	TBP yield (%)	TOF[b] (h^{-1})
1Al-ZSBA-1	1.1	30	0	0	29	0	0
3Al-ZSBA-1	2.6	45	71	32	5	3	0.30
5Al-ZSBA-1	4.8	50	76	38	4	3	0.19
5Al-ZSBA-1[c]	4.8	48	75	36	5	3	0.18
7Al-ZSBA-1	5.7	52	75	39	4	4	0.16
1Al-SBA-1-alk	1.0	37	0	0	36	0	0
3Al-SBA-1-alk	3.4	47	49	23	14	4	0.16
5Al-SBA-1-alk	5.5	53	60	32	5	6	0.14
5Al-SBA-1-alk[c]	5.4	52	60	31	6	6	0.14
7Al-SBA-1-alk	5.9	58	60	35	5	6	0.14
5Al-ZSM-5	5.0	28	72	20	2	3	0.10
Beta[d]	2	25	48	12	14	0	0.14

[a] Reaction conditions: 0.25 mmol DTBP, 0.25 mmol cinnamyl alcohol, 125 mg catalyst, 12.5 mL isooctane, 368 K, 5 h; [a]Measured by ICP-MS; [b] Based on flavan yield.; [c]Regenerated catalyst for second run; [d]CP814E, Zeolyst International

smaller than 1 nm, which obstacle the reactants from diffusing into the pores and accessing the acidic sites. Among the catalysts studied, 5Al-ZSBA-1 and 7Al-ZSBA-1 catalysts give the highest flavan yield around 38-39%, relatively high DTBP conversion of over 50%, and selectivity around 75% in the alkylation of DTBP with cinnamyl alcohol.

After the catalytic reactions, the 5Al-ZSBA-1 and 5Al-SBA-1-alk catalysts were regenerated by calcination at 823 K for 4 h. The regenerated catalysts were used under the same reaction conditions as that of the fresh catalysts, and the results are also listed in Table 7. The catalytic activities are well retained over both regenerated catalysts in the second run. Besides, no aluminium leaching occurred during the catalytic reaction based on Al/Si analysis by ICP-MS technique on the regenerated catalysts.

5. Conclusions

Aluminium incorporated cubic mesoporous silica of *Pm*3*n* phase was successfully synthesized using ZSM-5 seeds as the silica source and CTEABr as the template at pH around 9. The XRD patterns showed that well-ordered mesopores were retained with the Al/Si molar ratio up to 5% in the synthesis solution. Elemental analysis by ICP-MS showed that the amounts of Al(III) ions incorporated in the solids were close to those in the synthesis solutions up to Al/Si atomic ratio of 5%. From NH_3-TPD experiments, the acidic strength of Al-ZSBA-1 solids was higher than that of Al-SBA-1-alk samples, but lower than that of ZSM-5. Base on ^{27}Al MAS NMR, a high uniformity of Al in tetrahedral coordination was observed in Al-ZSBA-1 samples with Al/Si ratios up to 5% in the synthesis solutions.

The Al-incorporated cubic *Pm*3*n* mesoporous silica materials were efficient catalysts for the alkylation of DTBP by cinnamyl alcohol to yield flavan, and they showed higher catalytic activities than microporous Beta and ZSM-5 zeolites due to the facilitation of the diffusion of bulky reactant molecules in the mesopores. The highest activity was obtained over 5Al-ZSBA-1 and 7Al-ZSBA-1, assembled from zeolite seeds, which gave over 50% conversion and 38-39% flavan yield. The results demonstrate that Al-ZSBA-1 materials combine the advantages of strong acidity from zeolites and good diffusivity from mesoporous molecular sieves.

Acknowledgment

Financial supports from the Ministry of Science and Technology (NSC 101-2113-M-002-012-MY3) and Ministry of Education, Taiwan are gratefully acknowledged. Acknowledgments are also extended to Y.-Y. Yang, C.-Y. Lin, C.-Y. Chien, and Y.-C. Chao of Ministry of Science and Technology for SEM, TEM, and ICP-MS experiments.

Notes and references

1 A. Corma, *J. Catal.*, 2003, **216**, 298.
2 T. F. Degnan, *J. Catal.*, 2003, **216**, 32.
3 G. Sartori and R. Maggi, *Chem. Rev.*, 2006, **106**, 1077.
4 C. T. Kresge, M. E. Leonowicz, W. J. Roth, J. C. Vartuli and J. S. Beck, *Nature*, 1992, **359**, 710.
5 Q. S. Huo, D. I. Margolese, U. Ciesla, P. Y. Feng, T. E. Gier, P. Sieger, R. Leon, P. M. Petroff, F. Schüth and G. D. Stucky, *Nature*, 1994, **368**, 317.
6 A. Corma, *Chem. Rev*. 1997, **97**, 2373.
7 M. T. Janicke, C. C. Landry, S. C. Christiansen, S. B. Brirtalan, G. D. Stucky and B. F. Chmelka, *Chem. Mater.*, 1999, **11**, 1342.
8 R. Mokaya, *Angew. Chem. Int. Ed.*, 1999, **38**, 2930.
9 R. Ryoo, C. H. Ko and R. F. Howe, *Chem. Mater.*, 1997, **9**, 1607.

10 J. Cejka and S. Mintova, *Catal. Rev. -Sci. Eng.*, 2007, **49**, 457.
11 K. Egeblad, C. H. Christensen, M. Kustova and C. H. Christensen, *Chem. Mater.*, 2008, **20**, 946.
12 A. Corma, V. Fornes, J. M. Guil, S. Pergher, Th. L. M. Maesen and J. G. Buglass, *Micropor. Mesopor. Mater.*, 2000, **38**, 301.
13 K. Na, M. Choi and R. Ryoo, *Micropor. Mesopor. Mater.*, 2013, **166**, 3.
14 A. Karlsson, M. Stocker and R. Schmidt, Micropor. Mesopor. Mater., 1999, **27**, 181.
15 M. J. Verhoef, P. J. Kooyman, J. C. van der Waal, M. S. Rigutto, J. A. Peters and H. van Bekkum, *Chem. Mater.*, 2001, **13**, 683.
16 Y. Tao, H. Kanoh, L. Abrams and K. Kaneko, *Chem. Rev.*, 2006, **106**, 896.
17 Y. Liu, W. Zhang and T. J. Pinnavaia, *Angew. Chem. Int. Ed.*, 2001, **40**, 1255.
18 Y. Liu, W. Zhang and T. J. Pinnavaia, *J. Am. Chem. Soc.*, 2000, **122**, 8791.
19 P. -C. Shih, H. -P. Lin and C. -Y. Mou, *Stud. Surf. Sci. Catal.*, 2003, **146**, 557.
20 20 F. S. Xiao, *Top. Catal.*, 2005, **35**, 9.
21 P. Prokesova, S. Mintova, J. Cejka and T. Bein, *Micropor. Mesopor. Mater.*, 2003, **64**, 165.
22 X. Wang, X. Zhang, Y. Wang, H. Liu, J. Qiu, J. Wang, W. Han and K. L. Yeung, *Chem. Mater.*, 2011, **23**, 4469.
23 M. Ogura, S. Shinomiya, J. Tateno, Y. Nara, E. Kikuchi and M. Matsukata, *Chem. Lett.*, 2000, 882.
24 M. Ogura, S. Shinomiya, J. Tateno, Y. Nara, M. Nomura, E. Kikuchi and M. Matsukata, *Appl. Catal. A: General*, 2001, **219**, 33.
25 J. C. Groen, J. C. Jansen, J. A. Moulijn and J. Prez-Ramrez, *J. Phys. Chem. B*, 2004, **108**, 13062.
26 J. C. Groen, L. A. A. Peffer, J. A. Moulijn and J. Prez-Ramrez, *Chem. Eur. J.*, 2005, **11**, 4983.
27 C. J. H. Jacobsen, C. Madsen, J. Houzvika, I. Schmidt and A. Carlsson, *J. Am. Chem. Soc.*, 2000, **122**, 7116.
28 Z. Yang, Y. Xia and R. Mokaya, *Adv. Mater.*, 2004, **16**, 727.
29 J. -B. Koo, N. Jiang, S. Saravanamurugan, M. Bejblova, Z. Musilova, J. Cejka and S. -E. Park, *J. Catal.*, 2010, **276**, 327.
30 M. Choi, K. Na, J. Kim and Y. Sakamoto, O. Terasaki, R. Ryoo, *Nature*, 2009, **461**, 246.
31 M.E. Leonowicz, J.A. Lawton, S.L. Lawton, M.K. Rubin, *Science,* 1994, **24,** 1910.
32 W. J. Roth, P. Nachtigall, R. E. Morris and J. Cejka, *Chem. Rev.*, 2014, **114**, 4807.
33 W. J. Roth and J. Cejka, *Catal. Sci. Technol.*, 2011, **1**, 43.
34 K. Na, C. Jo, J. Kim, K. Cho, J. Jung, Y. Seo, R. J. Messinger, B. F. Chmelka and R. Ryoo, *Science*, 2011, **333**, 328.
35 Z. Zhang, Y. Han, F. S. Xiao, S. Qiu, L. Zhu, R. Wang, Y. Yu, Z. Zhang, B. Zou, Y. Wang, H. Sun, D. Zhao and Y. Wei, *J. Am. Chem. Soc.*, 2001, **123**, 5014.
36 Y. Liu and T. J. Pinnavaia, *Chem. Mater.*, 2002, **14**, 3.
37 D. P. Serrano, R. A. Garcia, G. Vicente, M. Linares, D. Prochazkova and J. Cejka, *J. Catal.*, 2011, **279**, 366.
38 Y. Hao, Y. Chong, S. Li and H. Yang, *J. Phys. Chem. C*, 2012, **116**, 6512.
39 P. J. Lebed, K. de Souza, F. Bilodeau, D. Lariviere and F. Kleitz, *Chem. Commun.*, 2011, **47**, 11525.
40 C. Pirez, J. -M. Caderon, J. -P. Dacquin, A. F. Lee and K. Wilson, *ACS Catal.*, 2012, **2**, 1607.
41 Q. Huo, D. I. Margolese and G. D. Stucky, *Chem. Mater.*, 1996, **8** 1147.
42 S. T. Hyde, *Pure Appl. Chem.*, 1992, **64**, 1617.
43 M. Kim and R. Ryoo, *Chem. Mater.*, 1999, **11**, 487.
44 M. Kruk, M. Jaroniec, R. Ryoo and J. M. Kim, *Chem. Mater.*, 1999, **11**, 2568.
45 A. Vinu, V. Murugesan and M. Hartmann, *Chem. Mater.*, 2003, **15**, 1385.
46 C.-C. Ting, H.-Y. Wu, Y.-C. Pan, S. Vetrivel, G. T. K. Fey and H. -M. Kao, *J. Phys. Chem. C*, 2010, **114**, 19322.
47 H.-M. Kao, C.-C. Ting, A. S. T. Chiang, C.-C. Teng and C. -H. Chen, *Chem Commun.*, 2005, 1058.
48 D. Ji, R. Zhao, G. Lv, G. Qian, L. Yan and J. Suo, *Appl. Catal. A: General*, 2005, **281**, 39.
49 A. Vinu, T. Krithiga, V. Balasubramanian, A. Asthana, P. Srinivasu, T. Mori, K. Ariga, G. Ramanath and P. G. Ganesan, *J. Phys. Chem. B*, 2006, **110**, 11924.
50 V. V. Balasubramanian, C. Anand, R. R. Pal, T. Mori, W. Böhlmann, K. Ariga, A. K. Tyagi and A. Vinu, *Micropor. Mesopor. Mater.*, 2009, **121**, 18.
51 R. Brzozowski, A. Vinu and B. Gil, *Appl. Catal. A: General*, 2010, **377**, 76.
52 M. -C. Liu, C. -S. Chang, J. C. C. Chan, H.-S. Sheu and S. Cheng, *Micropor. Mesopor. Mater.*, 2009, **121**, 41.
53 T. -H. Lin, C. -C. Chen, L. -Y. Jang, J. -F Lee and S. Cheng, *Micropor. Mesopor. Mater.*, 2014, **198**, 194.
54 T. R. Pauly, Y. Liu, T. J. Pinnavaia, S. J. L. Billinge and T. P. Rieker, *J. Am. Chem. Soc.*, 1999, **121**, 8835.
55 P.-G. Pietta, *J. Nat. Prod.*, 2000, **63**, 1035.
56 T. P. T. Cushnie and A. J. Lamb, *Int. J. Antimicob. Ag.*, 2005, **26**, 343.
57 E. Middleton; C. Kandaswami and T. C. Theoharides, *Pharmacol. Rev.*, 2000, **52**, 673.
58 S. J. Jong and S. Cheng, *Appl. Catal. A: General*, 1995, **126**, 51.
59 Q. Huo, D. I. Margolese, U. Ciesla, D. G. Demuth, P. Feng, T. E. Gier, P. Sieger, A. Firouzi, B. F. Chmelka, F. Schuth and G. D. Stucky, *Chem. Mater.*, 1994, **6**, 1176.
60 Y. Sakamoto, M. Kaneda, O. Terasaki, D. Y. Zhao, J. M. Kim, G. Stucky, H. J. Shin and R. Ryoo, *Nature*, 2000, **408**, 449.
61 S. Che, S. H. Lim,. M. Kaneda, H. Yoshitake, O. Terasaki and T. Tatsumi, *J. Am. Chem. Soc.*, 2002, **124**, 13962.
62 E. M. Flanigen, H. Khatami and H. Szymanski, *Adv. Chem. Ser.*, 1971, **101**, 201.
63 E. M. Flanigen, in J.A. Rabo (Editor), Zeolite Chemistry and Catalysis, Am. Chem. Soc., Washington, 1976, p. 80.
64 J. C. Jansen , F. J. van der Gaag and H. van Bekkum, *Zeolites*, 1984, **4**, 369.
65 G. Coudurier, C. Naccache and J. C. Vedrine, *J. Chem. Soc., Chem. Commun.*, 1982, 1413.
66 E. Oldfield, J. Haase, K. D. Schmitt and S. E. Schrammb, *Zeolites*, 1994, **14**, 101.
67 A. Corma, C. Corell, V. Fornes, W. Kolodziejski and J. Perez-Pariente, *Zeolites*, 1995, **15**, 576.
68 S. Zheng, H. R. Heydenrych, A. Jentys and J. A. Lercher, *J. Phys. Chem. B*, 2002, **106**, 9552.
69 B. Gil, S. I. Zones, S. -J. Hwang, M. Bejblova and J. Cejka, *J. Phys. Chem. C*, 2008, **112**, 2997.
70 X. Wang, S. Cheng and J. C. C. Chan, *J. Phys. Chem. C*, 2007, **111**, 2156.
71 D. Margolese, J. A. Melero, S. C. Christiansen, B. F. Chmelka and G. D. Stucky, *Chem. Mater.*, 2000, **12**, 2448.
72 J. Datka, S. Marschmeyer, T. Neubauer, J. Meusinger, H. Papp, F. -W. Schu1tze and I. Szpyt, *J. Phys. Chem.*, 1996, **100**, 14451.
73 A. Ungureanu, B. Dragoi, V. Hulea, T. Cacciaguerra, D. Meloni, V. Solinas and E. Dumitriu, *Micropor. Mesopor. Mater.*, 2012, **163**, 51.
74 Q. Yang, J. Yang, Z. Feng and Y. Li, *J. Mater. Chem.*, 2005, **15**, 4268.

Cubic *Pm3n* mesoporous aluminosilicate assembled from zeolite seeds as strong acidic catalysts

Tsung-Han Lin, Chia-Han Chen, Chi-Shuang Chang, Ming-Chang Liu, Shing-Jong Huang, and Soofin Cheng*

Department of Chemistry, National Taiwan University, Taipei 10617, Taiwan

Graphical Abstract

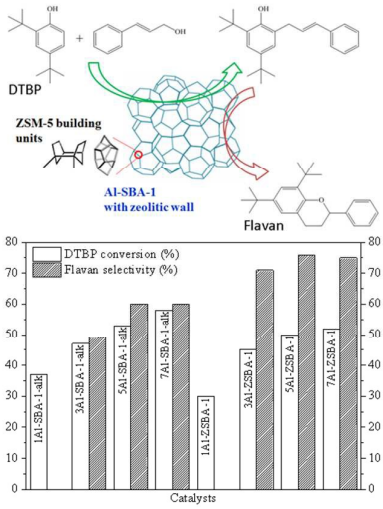

Cubic *Pm*3*n* mesoporous aluminosilicate with 3D interconnected pore structure, assembled with Al-incorporated ZSM-5 seeds at pH 9 using CTEABr as pore-directing agent, was an efficient catalyst in alkylation of 2,4-di-*tert*-butylphenol with cinnamyl alcohol to form flavan.